JOURNAL OF APPLIED ELECTROCHEMISTRY **27** (1997) 482–492

Interfacial pH measurement during the reduction of dissolved oxygen in a submerged impinging jet cell

C. DESLOUIS, I. FRATEUR*, G. MAURIN, B. TRIBOLLET

UPR 15 du CNRS, 4 pl. Jussieu, 75252 Paris, France

Received 22 January 1996; revised 19 September 1996

A pH sensor-grid assembly is used in a submerged impinging jet cell to measure the interfacial pH during the reduction of dissolved oxygen in well controlled flow conditions. Experiments were performed in a 0.5 M K_2SO_4 solution with and without carbonate ions. In each case a good agreement between experiment and theory is found. In particular it was confirmed that, in the absence of chemical reaction and for a totally mass transport controlled oxygen reduction reaction, stirring has no influence on the interfacial pH.

List of symbols

a	apparent rate constant introduced in Equation 10
a^*	hydrodynamic constant / dimensionless
A	surface area of the working electrode (m^2)
C_i	concentration of species i ($mol\,dm^{-3}$)
C_i^∞	bulk concentration of species i ($mol\,dm^{-3}$)
$C_i(0)$	concentration of species i at the electrode surface ($mol\,dm^{-3}$)
C^*	$= C_{HCO_3^-} + C_{CO_3^{2-}}, 2.2 \times 10^{-3}\ mol\,dm^{-3}$
d	nozzle diameter (m)
D_i	diffusion coefficient of species i ($cm^2\ s^{-1}$)
F	Faraday's constant ($96\,500\ C\,mol^{-1}$)
h	nozzle tip to electrode distance (m)
I_F	faradaic current (A)
I_l	limiting current (A)
k_1	rate constant in the forward direction for the homogeneous Reaction 8 ($cm^3\ mol^{-1}\ s^{-1}$)
k_{-1}	rate constant in the backward direction for the homogeneous Reaction 8 (s^{-1})
K_{eq}	equilibrium constant of carbonated species (Reaction 8) ($cm^3\,mol^{-1}$)
K_{H_2O}	water equilibrium constant (Reaction 15)
n	number of transferred electrons
N_i	flux density of species i ($mol\,cm^{-2}\,s^{-1}$)
$pH_1(0)$	interfacial pH on the first plateau of oxygen reduction
$pH_2(0)$	interfacial pH on the second plateau of oxygen reduction
R_i	homogeneous reaction rate of species i ($mol\,cm^{-3}s^{-1}$)
$\overline{U}$	average velocity at the nozzle exit ($m\,s^{-1}$)
v_z	velocity component in the axial direction ($m\,s^{-1}$)
z	axial coordinate (m)
z^*	$= z/\delta_{O_2}$ / dimensionless distance

Greek letters

α	numerical coefficient in Equation 1 / dimensionless
δ_i	thickness of the Nernst diffusion layer of species i (cm)
δ_r	thickness of the reaction layer (cm)
ν	kinematic viscosity of the electrolyte ($cm^2\,s^{-1}$)
Φ	diameter of the stagnation region (m)

Dimensionless groups

Re	Reynolds number, $\overline{U}d\,/\,\nu$
Re_L	Re value corresponding to the upper limit of the laminar flow regime
Re_T	Re value corresponding to the lower limit of the turbulent flow regime
Sc	Schmidt number, ν / D
Sh	Sherwood number

1. Introduction

The electrode/solution interfacial pH is different from the pH in the bulk of the solution when an electrochemical process is producing or consuming either hydronium or hydroxyl ions. Moreover, the interfacial pH shift caused by electrochemical reactions, can induce chemical reactions and produce soluble or insoluble species. For example, the interfacial pH increment due to hydrogen evolution during electrodeposition of metals such as nickel or iron can modify the electrochemical process and can even provoke the precipitation of colloidal hydroxide [1, 2]. pH change is also a central argument in theories of anomalous codeposition such as NiFe [3] or ZnCo [4]. Another example is afforded by the problem of scaling for-

* Also: Lyonnaise des Eaux - CIRSEE, 38 rue du Président Wilson, 78230 LE PECQ, France.

0021-891X

mation in seawater in particular on metallic surfaces under cathodic protection [5, 6, 7]. The cathodic reduction of dissolved oxygen, by increasing the interfacial concentration of OH^-, causes the precipitation of a solid deposit made of calcium carbonate and/or magnesium hydroxide, the critical pH values being 8.35 and 9.5 for each component [6].

These few examples show the great interest presented by experimental methods allowing the direct measurement of the interfacial pH in the presence of an electrochemical reaction. In particular, these methods should be very useful for optimizing the chemical treatments or additives which are proposed to prevent the scale precipitation. It is worth noting that in most cases the ionic or neutral species which are involved in the pH gradient are more or less under mass transport limitation. Therefore, it is necessary to perform this kind of measurements in well controlled hydrodynamic conditions.

Kuhn and Chan [8] reviewed the reliability of surface pH measurements during nickel electrodeposition using different techniques. Several methods of local pH measurement have already been developed for metal electrodeposition. Ovari and Rotinyan [9] used a microglass pH electrode to measure interfacial pH during nickel electrodeposition. Higashi *et al.* [4] used an antimony microelectrode to carry out similar investigations during zinc cobalt alloy electrodeposition. However, in all cases, the micro-sensors were introduced within the diffusion layer and disturbed the flow and potential fields at the very point of measurement.

Hessami and Tobias [10] designed a rotating ring-disc electrode where the ring electrode was used to evaluate the quantity of H^+ produced on the disk electrode during NiFe alloy codeposition. King *et al.* [11] measured the interfacial pH during oxygen reduction, with a Bi_2O_3 pH-sensing ring electrode. In these cases, hydrodynamics is well defined and the technique presents the advantage that the ring electrode does not interfere with the flow and the current distribution on the disc. However, the evaluation of the interfacial pH needs the knowledge in each case of the analytical expression of the protons transport towards the ring by taking into account the different homogeneous reactions.

A recent technique proposed by Romankiw [12] seems more attractive. In its original version a very thin mesh metallic grid, which is used as working electrode, is maintained in contact with the planar glass membrane of a pH electrode. The system is motionless. The pH of the small liquid volume contained in the holes of the grid is measured by the glass electrode. The variation of interfacial pH during NiFe codeposition was experimentally studied by this technique. Ji *et al.* [13] employed a similar set-up for the study of nickel electrodeposition. They also performed a few experiments by stirring the plating bath. They observed a significant effect on the pH due to the stirring but hydrodynamics was not sufficiently controlled to draw conclusions.

Recently, Deligianni and Romankiw [14] derived an improved variant of the original version by rotating the whole pH sensor-grid assembly. It was assumed that the flow pattern near the rotating grid electrode is similar to that of a rotating disc electrode. These authors showed that the measured interfacial pH is depending on the number of meshes of the Au or Ni grid and this dependence is decreasing with the current density. Then for high current density, a set of measurements with several mesh electrodes and different hole openings is necessary to obtain the surface pH value at the electrode by extrapolation. If the current density is low enough, this extrapolation seems less crucial. This device was used to investigate the Ni–Fe codeposition mechanism [14, 15].

The purpose of this paper is to describe a new experimental device allowing measurements of interfacial pH *in situ* under well-known flow conditions. It will be shown, that hydrodynamic conditions may have an influence on the interfacial pH. An electrochemical reaction which involves H^+ (or OH^-) ions and which is mass transport controlled has been chosen for assessing the interest of this technique. The reduction of dissolved oxygen in an aqueous solution containing an inert supporting salt, was first chosen to test the device because an analytical solution can be derived and the interfacial pH can be calculated. A second set of experiments was carried out in the presence of carbonate ions to study the effect of electrochemical /chemical coupled reactions on the interfacial pH. In both cases, experimental data were compared to an appropriate mathematical modelling.

The principle of this pH sensor is the same as that derived by Romankiw [12]. However, in contrast to the system described [12], it is based on the use of a motionless planar glass electrode/working grid electrode assembly, which needs no rotating electrical contacts. The hydrodynamics control is ensured by using a submerged impinging jet (SIJ) cell where the working electrode is uniformly accessible to mass transport.

2. Experimental details

The submerged impinging jet cell used in the present study was similar to that previously designed by Bouet *et al.* [16] and which was also used by Arkham *et al.* [17] to study nickel electrodeposition efficiency by *in situ* quartz crystal electrogravimetry with controlled hydrodynamics. The cylindrical vessel and the two flat plates were made of Plexiglass. The electrolyte jet was delivered by a cylindrical nozzle, impinging normally the planar electrode and spreading out radially over the bottom plate. The nozzle was made of a 25 cm long glass tube. According to various experimental investigations and in particular to direct measurements of the wall velocity gradient by electrodiffusion analysis [18], the diameter of the stagnation region, Φ, of the jet flow where the wall

surface is uniformly accessible is of the same order of magnitude as the nozzle diameter, d, for a laminar jet and depends, to a lower extent, on geometrical parameters of the cell. Consequently, a nozzle diameter, d, of 13 mm and a nozzle tip to electrode distance, h, of 20 mm were chosen in such a manner that the 12 mm diameter working electrode was uniformly accessible to mass transport.

The electrolyte jet was delivered from a two litre reservoir by means of a volumetric gear pump, the rotation rate of which was electronically controlled through a tachometer (Fig. 1).

The working electrode was a 82 mesh gold grid (Goodfellow, wire diameter: 0.06 mm, open area 64%). A 0.5 mm diameter gold wire, was welded on the periphery of the gold grid for electrical connection. The grid electrode with its electrical connection was contacted with the flat end of a combined pH electrode (Ingold, LOT 453-S7/110) and maintained on the lateral wall of the pH electrode with Teflon tape. The pH electrode/grid electrode assembly was fixed in the jet cell by means of a silicon glue to ensure watertightness of the setup. A large platinum grid used as counter electrode was fixed on the side opposite to the combined pH electrode and a saturated calomel electrode (SCE) was used as a reference electrode.

To ensure that the inner electrolytes of the combined pH electrode wetted the glass membrane and the annular porous frit, the SIJ cell was inclined at approximatively 45° (Fig. 1).

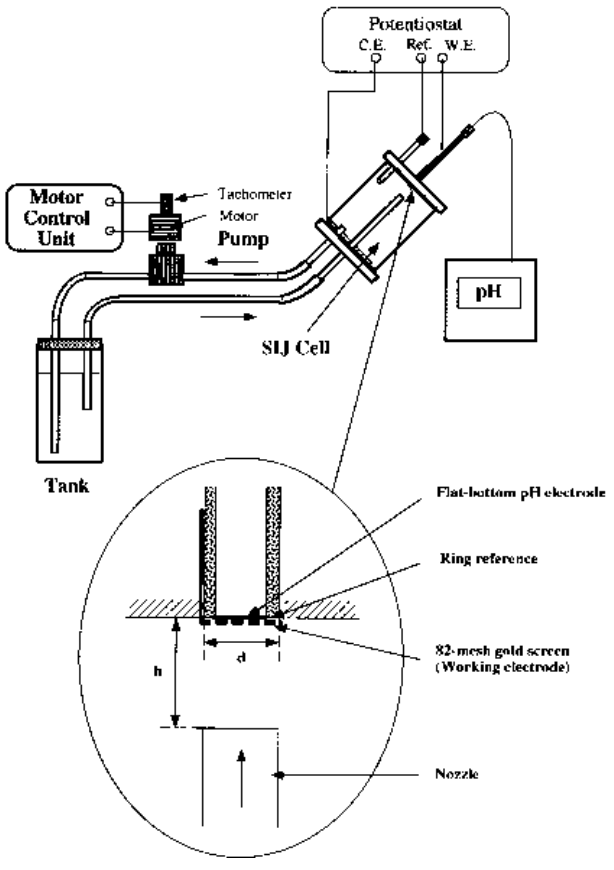

Fig. 1. Hydraulic and electrical circuit of the submerged impinging jet cell.

Two electrolytes were used: the first one was a 0.5 M K_2SO_4 solution and in the second one, 2×10^{-4} M Na_2CO_3 and 2×10^{-3} M $NaHCO_3$ were added. These carbonate concentrations correspond to that found in seawater, but sulfate supporting anions were preferred instead of chloride ones to avoid corrosion problems in the experimental device. All solutions were prepared with deionized water and high grade purity chemicals. The electrolytes were maintained in equilibrium with the atmosphere to ensure a constant oxygen concentration.

The potential of the grid electrode was monitored against the SCE with an electronic potentiostat (Sotelem) and a waveform generator (Hi-Tek Instruments). Before each set of experiments, the gold working electrode was prepolarized at –1 V vs SCE for several hours, in order to obtain thereafter reproducible results. The current–potential curves were plotted on a X–Y recorder (Sefram) with a sweeping rate of $2\,mV\,s^{-1}$. pH was simultaneously measured with a pH-meter (LPH 230T Radiometer). For a sudden pH change, the time response of the combined pH electrode equipped with the gold grid was about 1 min. Thus, when the potential was swept towards more negative values, the instantaneous measured pH was less than the steady state values and higher when the potential was swept in the reverse direction. However, on the oxygen reduction plateau where the current and concentrations remain practically constant for a long time, the instantaneous and steady values were identical.

3. Results

3.1. *Characterization of mass transfer in the SIJ cell*

The flow in the stagnation region of the impinging jet is axisymmetric, thus having close similarities with the flow near a rotating disk. Hence, Chin and Tsang [19] derived a semiempirical equation of mass transfer, which can be put in a dimensionless form as

$$Sh = \alpha Re^{1/2} Sc^{1/3} g(Sc) f(h/d) \qquad (1)$$

where the Sherwood number is proportional to the limiting current I_l following the definition:

$$Sh = \frac{I_l d}{nFAC^{\infty} D} \qquad (2)$$

Re is the Reynolds number based on the nozzle flow characteristics:

$$Re = \frac{\overline{U} d}{v} \qquad (3)$$

$\overline{U}$ is the average fluid velocity at the nozzle. $Sc = v/D$ is the Schmidt number and D the diffusion coefficient. α is a numerical coefficient depending on the tube geometry, on the flow regime (laminar or turbulent).

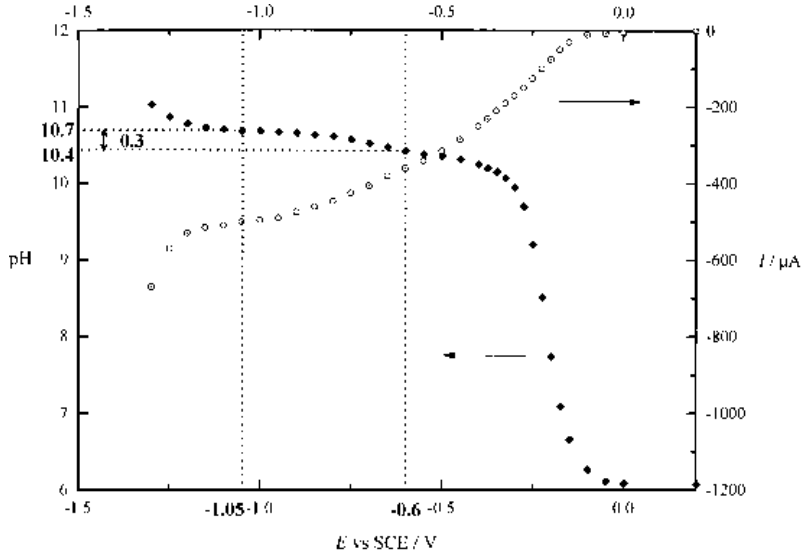

Fig. 2. Current-potential (○) and interfacial pH-potential (◆) curves for oxygen reduction in 0.5 M K_2SO_4 solution. $Re = 225$.

The f function expresses the dependence on the nozzle-to-plane distance, due to the interactions between the jet and the surrounding fluid at rest.

An example of steady state current–potential curve obtained with a 0.5 M K_2SO_4 solution is presented in Fig. 2. This curve is similar to that obtained previously for another electrolyte with a rotating disc electrode [20]. Two poorly resolved waves are observed: the first one around −0.6 V vs SCE and the second one around –1.05 V vs SCE. In [20], it is argued that the supporting electrolyte concentration influences the aspect of the current–potential curves, which indicates a great complexity of the oxygen reduction kinetics. According to Newman [21], for $5<pH<12$, oxygen reduction obeys the following two step mechanism:
first step:

$$O_2 + 2H_2O + 2e^- \Leftrightarrow H_2O_2 + 2OH^- \qquad (4)$$

second step:

$$H_2O_2 + 2e^- \longrightarrow 2OH^- \qquad (5)$$

The overall reaction is given by

$$O_2 + 2H_2O + 4e^- \longrightarrow 4OH^- \qquad (6)$$

Since Reaction 4 is generally faster than Reaction 5, hydrogen peroxide is a detectable and relatively stable intermediate [11]. For potentials more negative than $c.$ –1.2 V vs SCE, the absolute value of the current intensity increases rapidly due to the reduction of water molecules according to

$$2H_2O + 2e^- \longrightarrow H_2 + 2OH^- \qquad (7)$$

This last reaction is not under mass transport control at neutral or basic pH.

Figure 3 shows the variations of the limiting current measured at –1.05 V vs SCE versus the square root of the Reynolds number of the nozzle flow. As the less cathodic wave (Reaction 4) is poorly resolved, only the more cathodic one has been considered. In agreement with Equations 1 and 2, the limiting cur-

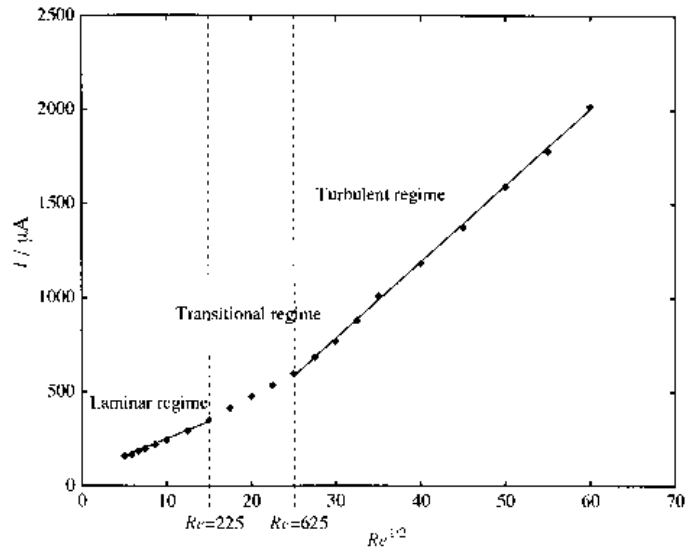

Fig. 3. Limiting current versus $Re^{1/2}$ in 0.5 M K_2SO_4 solution, on the second plateau of oxygen reduction (−1.05 V vs SCE).

rent is a linear function of the square root of *Re* in the laminar flow regime as well as in the transitional and turbulent ones. Thus the laminar domain corresponds to *Re* values less than $Re_L = 225$ and the turbulent flow regime begins at $Re_T = 625$. It is worth noting that the two limits Re_L and Re_T of the three hydrodynamic regimes are much smaller than the corresponding values determined by Bouet *et al.* on a planar disc electrode [16, 22]. They obtained $Re_L = 1400$ and $Re_T = 3000$ with a nozzle of 35 cm in length and 7 mm in diameter. They showed that the extent of the laminar regime was maximum for a tube length greater than 50 tube diameters. In the present work, the length to diameter ratio is only 19 which would partly explain the narrowness of the laminar domain. It is also worth noting that the extrapolated straight lines for the I_l vs $Re^{1/2}$ plots do not pass through the origin of the coordinates in the same way as in [16]. In particular, in the turbulent flow regime, the extrapolation to a zero *Re* value gives a negative value for the limiting current. These facts may be explained by the contribution to the current, of the inner part of the grid in contact with the stagnant solution between the grid and the glass membrane, mainly because mass transport contribution of this domain is determined by molecular diffusion. However, for our purpose it is enough that the system is mass transport controlled with a uniform current density, thus ensuring well-defined interfacial concentrations of the reacting or non-reacting species, even though the current density does not perfectly follow the equation valid for a smooth surface.

Therefore, except for the study of the flow rate influence on the interfacial pH, all experiments were carried out at the upper limit of the laminar flow regime ($Re = 225$).

3.2. *Interfacial pH increase due to electrochemical reduction of oxygen*

Figure 2 shows the variations of the interfacial pH during a potential sweep towards negative values, for a Reynolds number of 225. The interfacial pH increases from 6, which represents the bulk value, to 10.7 at the oxygen reduction plateau. The pH curve in fact exhibits two plateaux. The further pH increase for potentials less than –1.1 V vs SCE corresponds to the water reduction (Reaction 7), which contributes to a decrease of the proton concentration, but which is not mass transport controlled. It should be noted that both oxygen reduction plateaux, in particular that corresponding to Reaction 5, are far better defined on the pH–potential curve than on the corresponding current–potential curve. Therefore, the potential domains corresponding to Reactions 4 and 5 will be determined later from pH–potential curves.

The experimental value $pH_1(0)$ of the interfacial pH measured on the first plateau is 10.4 whereas on the second plateau $pH_2(0) = 10.7$. The difference between these two values equals $\log 2$. In agreement with Reactions 4 to 6, this result indicates that the overall reaction produces two times more hydroxyl ions than the first step. In the next section, this result will be theoretically justified.

Several pH–potential curves were plotted for different values of *Re* (Fig. 4). It appears that the interfacial pH is practically insensitive to electrolyte stirring on the second diffusion plateau (–1.05 V vs SCE), while a small influence is visible on the first plateau (–0.6 V vs SCE) and a more important one below the first plateau. For example, for *Re* varying over a very large range (25 to 1225), the variation of the interfacial pH on the second plateau does not exceed 0.03 pH (Fig. 5), a value within the limits of the experimental errors.

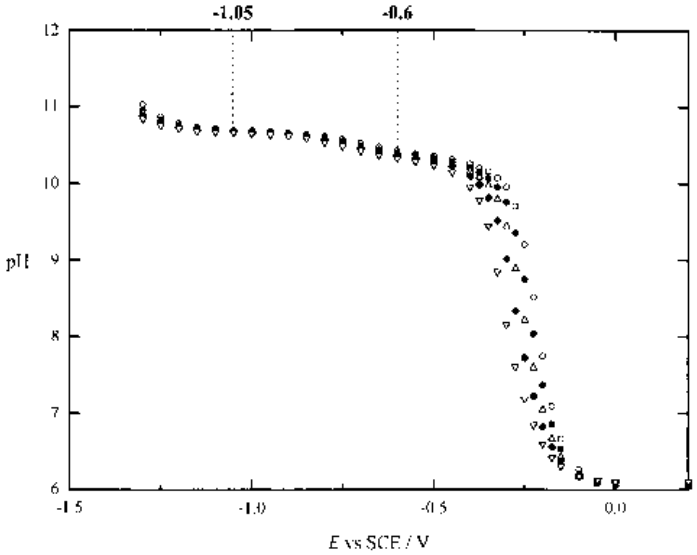

Fig. 4. Interfacial pH–potential curves for oxygen reduction in 0.5 M K_2SO_4 solution, at different Reynolds numbers: (○) $Re = 225$, (●) 400, (△) 625, (◆) 900 and (▽) 1225.

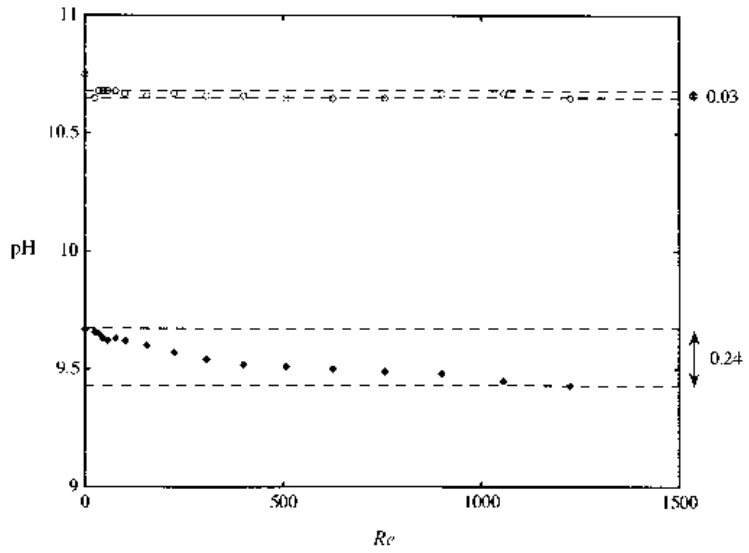

Fig. 5. Interfacial pH against Reynolds number on the second plateau of oxygen reduction, in 0.5 M K_2SO_4 (○) and the carbonated (◆) solution.

3.3. *Interfacial pH in the presence of carbonated species*

In the presence of carbonate, the OH^- ions produced by the electrochemical oxygen reduction Reactions 4 and 5 can be partially consumed by a chemical reaction involving HCO_3^- and CO_3^{2-} species dissolved in the electrolyte [6]:

$$OH^- + HCO_3^- \underset{k_{-1}}{\overset{k_1}{\Longleftrightarrow}} H_2O + CO_3^{2-} \qquad (8)$$

A buffering effect which reduces the pH increase in the vicinity of the cathodic interface can be expected.

In Fig. 6 the pH-potential curve obtained in the presence of carbonates for $Re = 225$ (laminar flow regime) is plotted. For the sake of comparison, the corresponding curve obtained in the absence of carbonates was also drawn. It should be noted that the plateau potentials, defined at the inflexion point on the current–potential curve, are slightly different from those in 0.5 M K_2SO_4 and equal –0.5 V vs SCE on the first plateau and –1 V vs SCE on the second one. The interfacial pH now starts from 8.3, reaches 9.3 on the first plateau and 9.6 on the second. The comparison of these values with those measured in the absence of carbonates emphasizes the buffering capacity of the carbonated solution. The HCO_3^-/CO_3^{2-} acid/base couple increased the pH of the bulk solution from 6 to 8.3 but it lowered the plateau value of the interfacial pH by about one pH unit. Here too, the difference between the two plateaux equals 0.3 pH unit. In Fig. 5, the variations of the interfacial pH with *Re* on the second plateau, obtained in the presence of carbonates, are also reported. At variance with the previous case, the pH plateau is no longer constant, but decreases by 0.24 pH unit when *Re* increases from 25 to 1225. A smaller variation of 0.1 pH unit is observed when the laminar flow only is considered ($25 < Re < 225$).

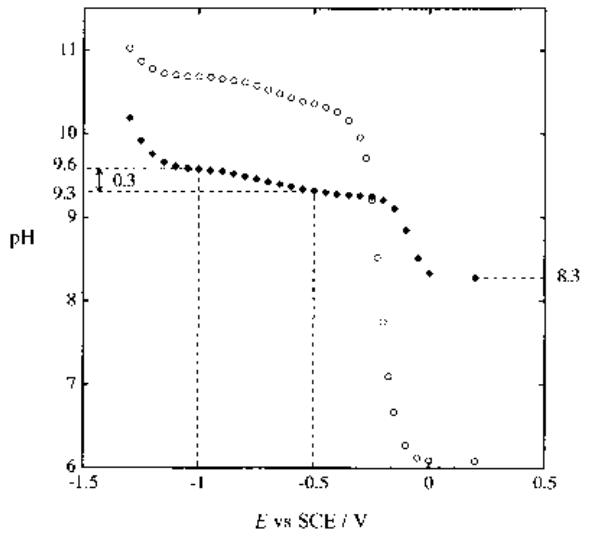

Fig. 6. Interfacial pH-potential curves for oxygen reduction in 0.5 M K_2SO_4 (○) and the carbonated (◆) solution $Re = 225$.

4. Modelling

4.1. *Purely electrochemical process*

On a gold electrode and in 0.5 M K_2SO_4, the reduction of dissolved oxygen is assumed to proceed in two steps (Reactions 4 and 5) giving two plateaux. The flux density of O_2 at the electrode surface is given in the Nernst approximation by

$$N_{O_2} = \frac{D_{O_2}}{\delta_{O_2}}\left(C_{O_2}^{\infty} - C_{O_2}(0)\right) \qquad (9)$$

where δ_{O_2} is the diffusion layer thickness of oxygen defined by convective diffusion.

This flux density is balanced by a kinetic flux:

$$N_{O_2} = a \times C_{O_2}(0) \qquad (10)$$

where a is an apparent rate constant depending on the potential.

Then, from Equations 9 and 10

$$C_{O_2}(0) = C^{\infty}_{O_2} \frac{1}{1 + a\,\delta_{O_2}/D_{O_2}} \qquad (11)$$

The fluxes conservation at the electrode wall can be written as

$$nN_{O_2} = N_{OH^-} = \frac{D_{OH^-}}{\delta_{OH^-}} \left[C_{OH^-}(0) - C^{\infty}_{OH^-}\right] \qquad (12)$$

where n, the number of transferred electrons, is 2 or 4 depending on whether Equation 4 or 6 is obeyed. The solution pH being equal to 6, $C^{\infty}_{OH^-}$ can be neglected.

In a SIJ cell, the diffusion layer thickness of species i is proportional to $D_i^{1/3} Re^{-1/2}$ according to [19]

$$\delta_i = 1.6386 \times D_i^{1/3} v^{-1/3} Re^{-1/2} \qquad (13)$$

Then, the interfacial OH^- concentration can be written as

$$C_{OH^-}(0) = nC^{\infty}_{O_2} \left(\frac{D_{O_2}}{D_{OH^-}}\right)^{2/3} \times \frac{1}{1 + D^{2/3}_{O_2}/1.6386 \times a v^{-1/3} Re^{-1/2}} \qquad (14)$$

4.1.1. Diffusion plateau conditions. In this case $a \to \infty$. Then, in Equation 14, the fraction depending on $Re^{-1/2}$ becomes equal to 1 and the interfacial concentration of OH^-, and therefore the interfacial pH, are independent of the fluid flow. For $n = 4$, this equation is in full agreement with the expression derived by Engell and Forchammer [5].

The parameters needed in the analytical calculation are listed in Table 1. It is noticed that the value of oxygen solubility $C^{\infty}_{O_2}$ measured in 0.5 M K_2SO_4 is in the usual range of values found for other electrolyte solutions [20]. At last the surface pH is related to the interfacial concentration of OH^- by the constant of the water equilibrium reaction:

$$H^+ + OH^- \Leftrightarrow H_2O \qquad (15)$$

with

$$K_{H_2O} = C_{H^+}(0) \times C_{OH^-}(0) = 10^{-14} \qquad (16)$$

Table 1. Diffusion coefficients and bulk concentrations of the components in both solutions, used in the model

Species	$D_i \times 10^5$ / $cm^2 s^{-1}$	C_i^{∞} / mol dm^{-3}
O_2	2*	2.2×10^{-4}†
OH^-	5.27‡	2×10^{-6}§
HCO_3^-	1.19‡	2×10^{-3}¤
CO_3^{2-}	0.955‡	2×10^{-4}¤

* Taken from [20].
† Calculated with the Levich equation from measurements performed on a rotating disc electrode.
‡ Taken from [23].
§ Only for the carbonated solution where the measured bulk pH is 8.3.
¤ Concentrations of carbonates introduced in the solution that correspond to equilibrium.

Thus for $n = 2, C_{OH^-}(0) = 2.3 \times 10^{-4}$ mol dm^{-3} which leads to an interfacial $pH_1(0)$ of 10.36. For $n = 4, C_{OH^-}(0) = 4.61 \times 10^{-4}$ mol dm^{-3} and therefore $pH_2(0) = 10.66$. The pH difference between the two plateaux is equal to $\log 2 \approx 0.30$ as found experimentally.

4.1.2. Below the plateau. The rate constant, a, has now a finite value. When Re becomes large, then

$$C_{OH^-}(0) \approx nC^{\infty}_{O_2} \frac{1.6386 \times a v^{-1/3} Re^{-1/2}}{D^{2/3}_{OH^-}} \qquad (17)$$

and the interfacial pH must decrease with increasing Re.

For a quantitative picture, close to the rest potential, $C^{\infty}_{OH^-}$ cannot be neglected with respect to $C_{OH^-}(0)$.

4.2. *Electrochemical / chemical process*

In this Section, the reduction of dissolved oxygen in the carbonated solution is considered. The OH^- production at the electrode surface disturbs the chemical equilibrium in the adjacent solution in a region called the kinetic or the reaction layer [24]. The concentration of each ionic species C_i is governed in the solution by the mass balance equation:

$$-\nabla N_i + R_i = 0 \qquad i = OH^-, HCO_3^- \text{ and } CO_3^{2-} \qquad (18)$$

By neglecting migration, the flux density N_i is

$$N_i = -D_i \nabla C_i + v_z C_i \qquad (19)$$

where v_z is the axial velocity component.

According to the chemical Reaction 8:

$$R_{OH^-, HCO_3^-} = k_{-1} C_{CO_3^{2-}} - k_1 C_{OH^-} C_{HCO_3^-} \qquad (20a)$$

and

$$R_{CO_3^{2-}} = -R_{OH^-} \qquad (20b)$$

The k_1 and k_{-1} rate constants, respectively, in the forward and the backward direction for Reaction 8, determine the equilibrium constant of carbonated species:

$$K_{eq} = \frac{k_1}{k_{-1}} = \frac{C^{\infty}_{CO_3^{2-}}}{C^{\infty}_{OH^-} C^{\infty}_{HCO_3^-}} \qquad (21)$$

In the present calculation, Reaction 8 is not assumed always to be at equilibrium near the electrode, contrary to the assumption used in [25, 26].

The following set of three one-dimensional equations can be written:

$$\begin{cases} -\nabla N_{OH^-} + R_{OH^-} = 0 & (22a) \\ -\nabla N_{OH^-} - \nabla N_{CO_3^{2-}} = 0 & (22b) \\ C_{HCO_3^-} + C_{CO_3^{2-}} = C^* & (22c) \end{cases}$$

If z is the axial coordinate, the boundary conditions of this system are as $z \to \infty$

$$C_{OH^-} = \frac{C^{\infty}_{CO_3^{2-}}}{K_{eq} C^{\infty}_{HCO_3^-}} \quad (23a)$$

$$C_{HCO_3^-} = C^{\infty}_{HCO_3^-} \quad (23b)$$

$$C_{CO_3^{2-}} = C^{\infty}_{CO_3^{2-}} \quad (23c)$$

at $z = 0$

$$\left.\frac{dC_{HCO_3^-}}{dz}\right|_{z=0} = \left.\frac{dC_{CO_3^{2-}}}{dz}\right|_{z=0} = 0 \quad (23d)$$

$$D_{OH^-}\left.\frac{dC_{OH^-}}{dz}\right|_{z=0} = \frac{I_F}{FA} \quad (23e)$$

where I_F is the faradaic current.

On the oxygen reduction plateaux, I_F is given by

$$I_F = -nFA\frac{D_{O_2}}{\delta_{O_2}} C^{\infty}_{O_2} \quad (24)$$

Equation 23(e) becomes

$$D_{OH^-}\left.\frac{dC_{OH^-}}{dz}\right|_{z=0} = -n\frac{D_{O_2}}{\delta_{O_2}} C^{\infty}_{O_2} \quad (25)$$

The velocity component in the axial direction v_z can be calculated in a SIJ cell from the semiempirical model of Chin and Tsang [19]:

$$v_z = -\frac{2 \times 0.656 \times (a^*)^{3/2}}{d^3} \nu Re^{3/2} z^2 \quad (26)$$

where a^* is a dimensionless hydrodynamic constant

For a uniform, laminar flow and for $1 \leq h/d \leq 3$:

$$a^* = 1.5852 - 0.76385(h/d) + 0.12926(h/d)^2 \quad (27)$$

In the present case, $h/d = 20/11$ and then $a^* = 0.62$.

Introducing a dimensionless distance z^* defined as z/δ_{O_2} and by taking into account Equations 26 and 13, Equations 22(a), (b) and (c) become

$$\frac{d^2 C_{OH^-}}{dz^{*2}} + \frac{2.1362\, D_{O_2}}{D_{OH^-}} z^{*2} \frac{dC_{OH^-}}{dz^*} + \frac{\delta^2_{O_2}}{D_{OH^-}} \times \left(k_{-1} C_{CO_3^{2-}} - k_1 C_{OH^-} C_{HCO_3^-}\right) = 0 \quad (28a)$$

$$\frac{d^2 C_{OH^-}}{dz^{*2}} + \frac{2.1362\, D_{O_2}}{D_{OH^-}} z^{*2} \frac{dC_{OH^-}}{dz^*} + \frac{d^2 C_{CO_3^{2-}}}{dz^{*2}} + \frac{2.1362\, D_{O_2}}{D_{CO_3^{2-}}} z^{*2} \frac{dC_{CO_3^{2-}}}{dz^*} = 0 \quad (28b)$$

$$C_{HCO_3^-} + C_{CO_3^{2-}} = C^* \quad (28c)$$

associated with the corresponding boundary conditions. Equation 25 takes the following form:

$$\text{at } z^* = 0 \qquad \left.\frac{dC_{OH^-}}{dz^*}\right|_{z^*=0} = -n\frac{D_{O_2}}{D_{OH^-}} C^{\infty}_{O_2} \quad (29)$$

Thus, in Equation 28a, the convection term (proportional to z^{*2}) is independent of stirring, whereas the chemical reaction one is proportional to $\delta^2_{O_2}$ so to Re^{-1}. In the same way, the boundary condition (29) is insensitive to stirring.

Equations 28(a), (b) and (c) were numerically solved by using Newman's method [21, 27] allowing the treatment of coupled, non-linear ordinary differential equations. The computer program written for that use does not only give the interfacial pH but also the concentration profiles of OH^-, HCO_3^- and CO_3^{2-} species.

It should be noted that by solving Equation 28(a) where the chemical reaction term ($k_{-1} C_{CO_3^{2-}} - k_1 C_{OH^-} C_{HCO_3^-}$) is set to zero, an interfacial pH value identical to that previously analytically found for a 0.5 M K_2SO_4 solution is found.

The values of the different parameters used in the model are listed in Tables 1 and 2. It is mentioned that the value of K_{eq} calculated analytically is close to $K_{eq} = 0.84 \times 10^8\ cm^3\ mol^{-1}$, predicted from the equations of Skirrow [28]. One important point is that whereas the numerical value of K_{eq} is well known [28], the effective value of k_1 and k_{-1} were never determined and consequently in [25, 26], Reaction 8 is considered at equilibrium. For this reason, we solved the differential equations for a large range of k_1. The boundary conditions for $z \to \infty$ are then applied at the distance $z^* = 5$.

The calculated values of $pH_2(0)$ are reported in Fig. 7 as a function of Re for $10^2 \leq k_1 \leq 10^{12}\ cm^3\ mol^{-1}\ s^{-1}$. For $pH_1(0)$, the numerical derivation gives values 0.3 pH unit below $pH_2(0)$ values.

It is noticed that for very small or very large k_1, the interfacial pH is independent of Re, whereas, for intermediate values ($10^6 \leq k_1 \leq 10^8\ cm^3\ mol^{-1}\ s^{-1}$) the interfacial pH is increased by approx. 0.7 pH unit when Re varies from 25 to 1225. For small values of k_1($10^2\ cm^3\ mol^{-1}\ s^{-1}$), the interfacial pH is the same as that in 0.5 M K_2SO_4 solution ($pH_2(0)$ 10.66). When k_1 increases at constant Re, $pH_2(0)$ decreases and reaches the limiting value of 8.73.

5. Discussion

5.1. *Oxygen reduction in a neutral electrolyte*

The agreement between the experimental and predicted pH values is excellent for the two plateaux of oxygen reduction. The measured values of 10.4 and 10.7 are very close to the calculated values of 10.36 and 10.66, respectively, and their difference of 0.3 pH unit is consistent with two successive reactions exchanging two electrons each.

Table 2. Other parameters in the model

Parameter	*Value*
ν	$10^{-2}\ cm^2\ s^{-1}$
K_{eq}	$0.5 \times 10^8\ cm^3\ mol^{-1}$[§]
C^*	$2.2 \times 10^{-3}\ mol\ dm^{-3}$

[§]Calculated from Equation 21.

It is interesting to note that the pH–potential curve which corresponds only to the reduction of oxygen is clearer and easier to analyse than the current–potential curve. To date, the only measurement of the peroxide oxidation on the ring electrode of a ring disc electrode device was able to assess the potential range corresponding to each reaction (Reactions 4 and 5) [11]. The absence of the stirring effect on the plateaux is also experimentally obvious and in agreement with the theory and of course independent of the flow geometry. The interfacial pH is only function of the potential and the oxygen concentration. On the contrary, below the plateaux, Fig. 4 shows an influence of stirring on the interfacial pH. In qualitative agreement with Equation (14), it can be verified that for a constant overpotential, the interfacial pH decreases when *Re* increases.

However, the absolute values of the plateaux currents, especially that corresponding to the exchange of four electrons, which is well-defined, are significantly higher than the values calculated from the theoretical expression deduced from the combination of Equations 1 and 2. That is,

$$I_l = \frac{nFAC^{\infty}D}{d}\alpha Re^{1/2}Sc^{1/3} \qquad (30)$$

with $g(Sc)$ and $f(h/d) \approx 1$ and $\alpha \approx 0.67$ [19].

For example, a plateau current value of 170 μA is calculated instead of the actual value of about 500 μA measured at $Re = 225$ (Fig. 2). A possible explanation of this effect, which must be analysed together with the apparent narrowness of the laminar regime mentioned earlier, is that the actual area, A, is not known and, due to the mesh characteristics (wire diameter 60 μm and mesh period 310 μm), mass transport can be notably enhanced by the roughness of the grid. At low Reynolds numbers, the mass flux is just affected by a proportionality factor which corresponds to an increase of the apparent area *A*. Therefore, the low *Re* value for the higher limit of the laminar flow probably marks the transition with a different mass transport domain but does not correspond to the onset of turbulent flow.

This drawback could be eliminated with an electroformed very thin metal screen. In this case a good agreement must exist between the interfacial pH value and the oxygen reduction current (Equation 12). The number of meshes necessary for this kind of comparison is very large [14]. Fortunately the aim of this work is to measure the pH at the interface and not to analyse quantitatively the current.

5.2. *Oxygen reduction in a buffer solution*

The equilibrium between carbonate species (Reaction 8) has a buffering effect, and consequently the variation of pH against potential occurs in a smaller range than in a non-reacting neutral electrolyte (Fig. 6). This result is in agreement with the results presented by King *et al.* [11] even if in their case the pH variation is much smaller than in the present work.

To understand the difference between our results and those of King *et al.* [11], it is necessary to consider the thickness of the reaction layer defined from Equation 28(a), following the same procedure as described by Levich [24], by

$$\delta_r = \sqrt{\frac{D_{OH^-}}{k_1 C_{HCO_3^-} + k_{-1}}} \qquad (31)$$

For low k_1 values (lower than 10^3 cm^3 mol^{-1} s^{-1}), δ_r is very large with respect to the diffusion layer thickness and the chemical reaction consumes almost no OH^- in the diffusion layer. The corresponding term in Equation 28(a) is negligible with respect to the diffusion and convective terms and the stirring has no influence on the interfacial pH. Its value is that one calculated for an ordinary neutral electrolyte (~10.66).

For intermediate k_1 values (10^6 to 10^8 cm^3 mol^{-1} s^{-1}), the thickness of the reaction layer and the thickness of the diffusion layer are on the same order of magnitude, then stirring influences the interfacial pH value which is an intermediate between the two extrema: 10.66 and 8.73. As a consequence, the k_1 value can be determined by comparison of the experimental results with the numerical data. It has been found that $k_1 \approx 10^7$cm^3 mol^{-1} s^{-1}. Theoretically the interfacial pH increases with the Reynolds number (Fig. 7) and experimentally a slight decrease is observed (Fig. 5). This difference can be due to the fact that the thickness of the grid is not negligible (60 μm) and then, a motionless volume of solution is trapped in the holes of the grid. Therefore, in the case of a buffering effect, the chemical equilibrium is not disturbed in the same way in the motionless volume and in the stirred solution. However, the discrepancy between experiments and theory is only two tenths of a pH unit when the analysis is restricted to the laminar flow ($Re < 225$). For these intermediate k_1 va-

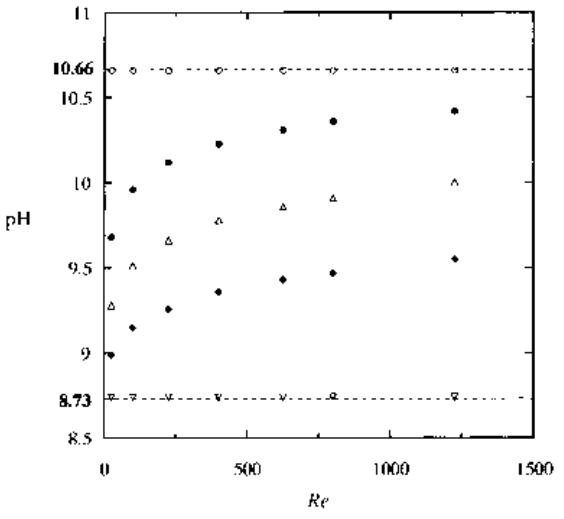

Fig. 7. Evolution of theoretical interfacial pH with Reynolds number in the carbonated solution, on the second plateau of oxygen reduction ($E = -1$ V vs SCE), for different values of k_1 : (○) $k_1 = 10^2$, (●) 10^6,(△) 10^7, (◆) 10^8 and (▽) 10^{12}) cm^3 mol^{-1} s^{-1}. Each point corresponds to a numerical integration of Equations 28.

lues, δ_r is lower than δ_{OH^-} while keeping in the same order of magnitude. In Fig. 8(a), the values of δ_r/δ_{O_2} can be obtained from the extrapolation of the wall concentration profiles and these values are in good agreement with Equation 31.

For high k_1 values (larger than 10^{12} $cm^3 mol^{-1} s^{-1}$), δ_r tends towards zero and Reaction 8 is strictly at equilibrium (Equation 21) everywhere in the solution. In the set of three coupled differential Equations 28(a), (b) and (c), Equation 28(a) is replaced by Equation 21, where the concentrations are the local ones. The stirring effect disappears and the interfacial pH becomes independent of the flow. Its value is determined by the value of K_{eq}. The calculated concentration profile is given in Fig. 8(b) on a more appropriate scale than in Fig. 8(a). It then appears that the zoomed out interfacial pH is still different from the bulk pH. Moreover the boundary layer condition (Equation 29) fixed the concentration gradient at the interface ($z^* = 0$). Its value is different from the concentration gradient near the electrode ($z^* \neq 0$), this last gradient being mainly determined by the convective diffusion process (Fig. 8(b)).

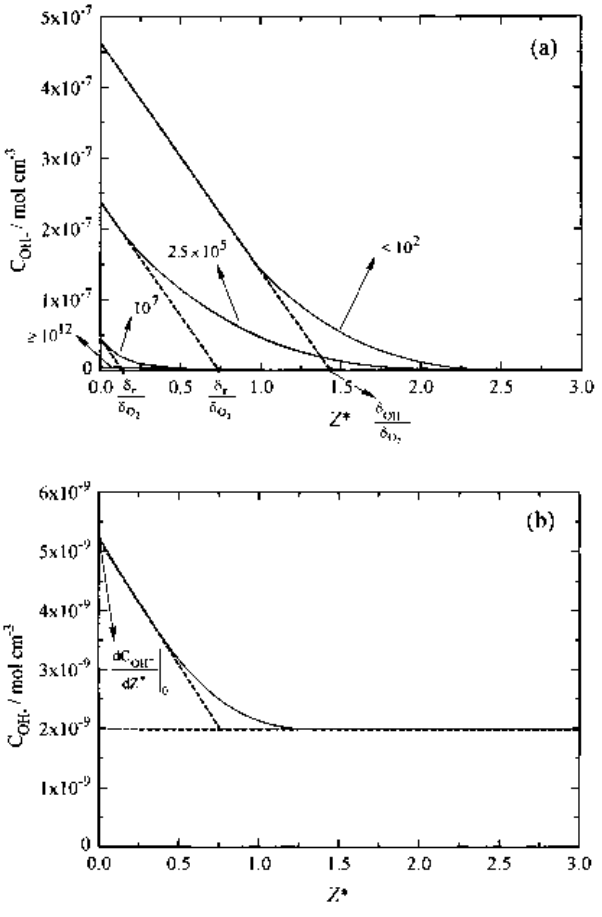

Fig. 8. Calculated concentration profiles with carbonated species, on the second plateau of oxygen reduction ($E = -1$ V vs SCE), for different values of k_1. The dimensionless coordinate z^* is defined as z/δ_{O_2} where δ_{O_2} is the diffusion layer thickness of oxygen. $Re = 225$. (a) Each curve corresponds to a particular value of k_1, given in $cm^3 mol^{-1} s^{-1}$. (b) $k_1 \geq 10^{12} cm^3 mol^{-1} s^{-1}$, same curve as in Fig. 8(a) with a different scale.

6. Conclusion

A special device for measuring the interfacial pH in the course of an electrochemical reaction has been built-up by assembling a grid electrode and a pH glass electrode, following an original idea of Romankiw [12]. It was tested in the case of oxygen reduction without or with carbonated species simulating the prerequisite conditions for calcareous deposit.

A straightforward analytical solution, in the former case, and a numerical solution in the latter case were derived for the interfacial pH. Experimental verification was performed using a submerged impinging jet cell which ensured a quantitative hydrodynamic control. The experimental and theoretical interfacial pH were in good agreement in the absence of carbonated species. It was also confirmed that stirring has no influence on this parameter as predicted from calculation. From the comparison of the measured and simulated pH in the presence of carbonated species, an estimate of the forward rate constant of the chemical reaction consuming hydroxyl ions could be given.

Acknowledgements

This work was supported financially by La Lyonnaise des Eaux – CIRSEE, 38 rue du Président Wilson, 78230 Le Pecq.

References

[1] L. B. Harris, *J. Electrochem. Soc.* **120** (1973) 1034.
[2] S. K. Verma and H. Wilman, *J. Phys. D: Appl. Phys.* **4** (1971) 2051.
[3] H. Dahms and L. M. Croll, *J. Electrochem. Soc.* **112** (1965) 771.
[4] K. Higashi, H. Fukushima and T. Urakawa, *J. Electrochem. Soc.* **128** (1981) 2081.
[5] H. J. Engell and P. Forchammer, *Corros. Sci.* **5** (1965) 475.
[6] G. Philipponneau, Thèse de Docteur Ingénieur, Ecole Centrale des Arts et Manufactures, Paris (1982).
[7] W. Hart, C. Culberson and S. Smith, *Corrosion NACE* **40** (1984) 609.
[8] A. T. Kuhn and C. Y. Chan, *J. Appl. Electrochem* **13** (1983) 189.
[9] E. Ovari and A. I. Rotinyan, *Sov. Electrochem.* **6** (1970) 516.
[10] S. Hessami and C. W. Tobias, *AIChE J.* **39** (1993) 149.
[11] F. King, C. D. Litke and Y. Tang, *J. Electroanal. Chem.* **384** (1983) 189.
[12] L. T. Romankiw, Proceedings of the Symposium on 'Electrodeposition Technology, Theory and Practice'. (edited by L. T. Romankiw and D. R. Turner), The Electrochemical Society, NJ (1987), *87-17*, p. 301.
[13] J. Ji, W. C. Cooper, D. B. Dreisinger and E. Peters, *J. Appl. Electrochem.* **25** (1995) 642.
[14] H. Deligianni and L. T. Romankiw, IBM *J. Res. Develop.* **37** (1993) 85.
[15] P. C. Andricacos and L. T. Romankiw, *in* 'Advances in Electrochemical Science and Engineering' vol:3, (edited by H. Gerischer and C. W. Tobias), VCH, Weinheim (1994), pp. 227–322.
[16] V. Bouet, C. Gabrielli, G. Maurin and H. Takenouti, *J. Electroanal. Chem.* **340** (1992) 325.
[17] C. Arkham, V. Bouet, C. Gabrielli, G. Maurin and H. Perrot, *J. Electrochem. Soc.* **141** (1994) L103.
[18] F. Baleras, C. Deslouis, B. Tribollet and V. Sobolik, *J. Appl. Electrochem.* **24** (1994) 676.

[19] D. -T. Chin and C. -H. Tsang, *J. Electrochem. Soc.* **125** (1978) 1461.
[20] C. Deslouis, O. Gil, B. Tribollet, G. Vlachos and B. Robertson, *J. Appl. Electrochem.* **22** (1992) 835.
[21] J. Newman, 'Electrochemical Systems', 2nd edn., Prentice-Hall, Englewood Cliffs, NJ (1991).
[22] V. Bouet, Thèse de Doctorat, Université Pierre et Marie Curie, Paris (1994).
[23] Y. -H. Li and S. Gregary, *Geochim. Cosmochim. Acta* **38** (1974) 703.
[24] V. G. Levich, 'Physicochemical Hydrodynamics', Prentice-Hall, Englewood Cliffs, NJ (1962).
[25] J. F. Yan, T. V. Nguyen, R. E. White and R. B. Griffin, *J. Electrochem. Soc.* **140** (1993) 733.
[26] J. F. Yan, R. E. White and R. B. Griffin, *ibid* **140** (1993) 1275.
[27] J. Newman, *Ind. Eng. Chem.* **7** (1968) 514.
[28] G. Skirrow, *in* 'Chemical Oceanography', vol.2, 2nd edn., (edited by J. P. Riley and G. Skirrow), Academic Press, New York (1975).